Two Active X-chromosomes Modulate the Growth, Pluripotency Exit and DNA Methylation Landscape of Mouse Naive Pluripotent Stem Cells through Different Pathways

Juan Song[1], Adrian Janiszewski[1], Natalie De Geest[1], Lotte Vanheer[1], Irene Talon[1], Taeho Oh[1], Vincent Pasque[1,*].

[1] KU Leuven - University of Leuven, Department of Development and Regeneration, Herestraat 49, B-3000 Leuven, Belgium.

[*] Correspondence to: vincent.pasque@kuleuven.be (V.P.)

Format: Research paper

ABSTRACT

Sex is an increasingly important feature of mouse naive pluripotent stem cells (PSCs), but the regulatory processes involved remain enigmatic. Here, we addressed how sex modulates pluripotency by characterizing the transcriptional state, differentiation dynamics, growth and DNA methylation in female ESCs with heterozygous deletions of *Dusp9*. Our results show that sex-specific regulation of DNA methylation by *Dusp9* can be molecularly uncoupled from the regulation of sex-specific differences in growth, transcription and pluripotency exit. We also addressed how sex modulates pluripotency by characterizing, in male and female cells, the transcriptional state and differentiation dynamics of iPSCs. We found that iPSCs adopt distinct sex-specific transcriptional states, pluripotency exit kinetics and growth properties, which correlate with the presence of two active X chromosomes. Differences in growth and pluripotency exit are not explained by X-linked pluripotency genes. We also examined the open chromatin landscape of embryonic stem cells (ESCs). Epigenomic profiling revealed sex-specific open chromatin landscapes associated with pluripotency and development that underlie key pluripotency and signaling transcription factor binding sites. The differential enrichment of binding sites in sex-specific open chromatin regions provides a molecular link between transcriptional regulators, maintenance of and exit from pluripotency. Our results uncover that different pathways regulate distinct sex-specific differences in PSCs and reveal new molecular insights on sex-specific cellular states.

INTRODUCTION

Pluripotent stem cells (PSCs) are important for modeling development and diseases and for the design of future regenerative medicine approaches [1]. A key question in the field is what mechanisms underlie the establishment and maintenance of pluripotency. Somatic cells can be reprogrammed into induced PSCs (iPSCs) by transcription factor overexpression [2] and mouse embryonic stem cells (ESCs) can be derived directly from early embryos [3]. Both cell types have the capacity to self-renew and maintain embryonic lineage differentiation potential in culture [4]. It is of outstanding interest to understand what epigenetic and genetic mechanisms influence the molecular and functional properties of PSCs.

Increasing evidence suggests that X-chromosome dosage can modulate the molecular and functional properties of mammalian PSCs [5–16]. Female cells undergo X-chromosome reactivation in the mouse inner cell mass resulting in two active X-chromosomes (XaXa), a state maintained in female ESCs and induced by reprogramming to iPSCs [17–19], reviewed in [20]. XaXa is a hallmark of mouse naive pluripotency, the latter is characterized by unbiased embryonic lineage differentiation potential. Consequently, XX mouse naive PSCs have a double dose of X-linked genes and an increased X-to-autosome gene expression ratio compared with XY cells. Work over the past decade showed that female ESCs exhibit global DNA hypomethylation affecting most genomic features including imprint control regions [9–16,21]. Recent work showed that female iPSCs also display global hypomethylation [22]. Differences in global DNA methylation have been attributed to X-chromosome dosage since female XO cells display male-like DNA methylation levels [9,11,13]. Female ESCs and iPSCs have genetically unstable X-chromosomes, deleting part or whole X-chromosomes [9,11,13–15,23,24]. Thus, mouse ESCs and iPSCs show DNA methylation and genetic loss of one X chromosome associated with XaXa.

It was also discovered by the Heard group that female XX ESCs show increased expression of several pluripotency-associated mRNAs, and display delayed pluripotency exit, indicating that features of naive pluripotency are promoted in female XX ESCs [11,25]. Differences in transcription have also been attributed to X-chromosome dosage since female XO ESCs, or *Xist*-induced X-chromosome inactivation, are associated with male-like pluripotency-associated gene expression and pluripotency exit [11]. Therefore, it is important to determine the potential influence of X-chromosome dosage on the molecular and functional properties of iPSCs and also for mechanistic studies of reprogramming. Despite its importance, a systematic comparison of transcriptional states and pluripotency exit in male and female mouse iPSCs has not yet been performed.

While several advances have been made, the molecular pathways by which XaXa modulate pluripotency remain incompletely understood [6]. At the mechanistic level, two active X-chromosomes inhibit MAPK and GSK3 signaling [8,11], and global DNA hypomethylation has been attributed to reduced expression of DNMT3A and DNMT3B [9], or DNMT3L [10], or UHRF1 [13,15,22] in female ESCs/iPSCs. More recently, it was discovered that increased dosage of the X-linked MAPK inhibitor *Dusp9* (dual-specificity phosphatase 9) is in part responsible for inhibiting DNMT3A/B/L and global DNA hypomethylation in female ESCs [13].

The expression level of *Dusp9* is higher in XX ESCs than in XY ESCs and overexpression of *Dusp9* in male ESCs induced female-like global DNA hypomethylation. Conversely, heterozygous deletion of *Dusp9* in female ESCs restored male-like global DNA methylation, suggesting that *Dusp9* is responsible for MAPK-mediated DNMT3A/B repression in female ESCs. However, whether *Dusp9* heterozygous deletion in female ESCs has effects on the transcriptional regulatory network and pluripotency exit has not yet been explored. Furthermore, how and which X-linked genes modulate the pluripotency regulatory network of naive PSCs remains unclear [6]. In addition, novel insights may be gained by identification of cis-regulatory elements that drive sex-specific pluripotent stem cell states.

Here, in order to investigate the influence of X-chromosome dosage on iPSCs, we systematically compared male and female mouse iPSCs at different passage and at the transcriptional, pluripotency exit, cell growth and X-chromosome dosage level. We found that sex-specific differences in cell growth, transcription and pluripotency exit are established late during iPSC reprogramming and subsequently resolved as a result of X-chromosome loss in female iPSCs upon passage. We further investigated the regulatory landscape of male and female ESCs using genome-wide chromatin accessibility analyses. We found that thousands of chromatin regions differ in accessibility in male and in female ESCs. Motif discovery analysis identified that more accessible chromatin in female ESCs is enriched for binding sites of key pluripotency regulators including KLF/ESRRB/OCT4/SOX2, suggesting stabilization of the naive pluripotency regulatory network via these regulators. By contrast, chromatin sites more accessible in male ESCs are most enriched for AP-1/TEAD motifs, downstream effectors of singaling pathways including MAPK and Hippo. We show that XY ESCs grow faster than XX ESCs, irrespective of culture conditions, mimicking growth differences between male and female mammalian post-implantation embryos. We further demonstrate that delayed exit from pluripotency and female-like transcription is maintained in the presence of male-like global DNA methylation in *Dusp9* heterozygous female ESCs. Altogether, we provide a previously unrecognized view of sex-specific epigenetic and transcriptional states and regulation in female naive PSCs, as well as chromatin accessibility landscapes and their associated transcriptional regulators, setting the stage for studying gene regulatory networks that are modulated by X-chromosome dosage in PSC.

RESULTS

Characterization of Cell Growth, Transcriptional States, and Pluripotency Exit in Male and Female iPSCs

In order to explore the importance of sex on cell growth, transcriptional states and pluripotency exit of mouse iPSCs, we derived male and female iPSC lines from isogenic mouse embryonic fibroblasts (MEFs) carrying a tetO inducible transgene encoding the reprogramming factors *Oct4, Sox2, Klf4* and *c-Myc* in the *Col1A* locus and the reverse tetracycline transactivator (M2rtTA) in the *Rosa26* locus (Figure 1A) [26]. After two weeks of doxycycline (dox) treatment to induce reprogramming, 10 female and 11 male iPSC lines were expanded on feeders in the presence of serum and LIF (S/L) in the absence of dox (Figure 1A), or adapted to dual

ERK/GSK3 inhibition and LIF conditions (2i/L) (Figures S1A-E). This scheme allowed us to directly compare female and male iPSCs without the influence of differences in genetic background, reprogramming system or derivation method. Both female and male iPSCs could be propagated over multiple passages while maintaining their morphology, indicative of self-renewal, and expressed pluripotency-associated factors NANOG and DPPA4 (Figures 1B, S1A-B). Female iPSCs reactivated the inactive X-chromosome (Figures S1C/D), a marker of naive pluripotency [27]. Thus, we derived isogenic male and female iPSCs.

We asked whether sex affects iPSCs growth. We counted the number of male and female iPSCs over two days starting from the same amount of cells. We found that all our early passage female iPSC lines grew slower than male iPSCs, with a doubling time (Td) extended by ˜3.4 hours compared with male iPSCs grown in S/L (Td female=18.4.±1.5hr vs Td male=15.0±0.9hr) (Figure 1C). Similarly, we found that female ESCs grew slower than male ESCs (Figure 1C). The sex-specific difference in iPSCs and ESCs growth did not depend on culture conditions because female ESCs and iPSCs still grew slower than male cells in 2i/LIF (Figure S1F). We conclude that early passage female mouse PSCs are characterized by lower growth compared with their male counterparts. These results are in agreement with the documented growth delay of female mammalian post-implantation embryos compared to male embryos [28].

Using reverse transcription (RT) quantitative real-time PCR (qPCR) we found that in S/L, all our early passage female iPSC lines consistently expressed higher levels of pluripotency-associated genes *Prdm14*, *Nanog* and *Tcl1* compared with male iPSCs (Figure 1D). Western blot analysis showed that female iPSCs had increased NANOG protein levels compared with male iPSCs (Figure 1E). These differences closely resemble those of mouse ESCs [11,13], in agreement with the notion that iPSCs are molecularly equivalent to ESCs. Thus, reprogramming to iPSCs results in sex-specific differences in pluripotency-associated gene expression.

Next, prompted by the differences in pluripotency gene expression, we investigated the extent to which sex affects exit from pluripotency in iPSCs. We subjected female and male iPSCs to LIF withdrawal-mediated differentiation and measured the downregulation of pluripotency-associated genes by RT-qPCR. Exit from pluripotency was delayed in female iPSCs for *Prdm14*, *Nanog* and *Tcl1* (Figure 1F). We confirmed these results using an alternative differentiation protocol that mimics epiblast differentiation (Figures S1E, S1G-I) [11,29]). Thus, female iPSCs exit pluripotency with delayed kinetics compared with male iPSCs, consistent with previous studies in ESCs [11,25]. Altogether, these findings show that our newly derived early passage iPSCs display sex-specific behavior in growth, pluripotency gene expression and in pluripotency exit kinetics, recapitulating sex-specific differences in mouse embryos and ESCs [11,28].

Differences in Cell Growth, Transcription and Pluripotency Exit Correlate with the Presence of Two Active X-chromosomes

Female XX ESCs are prone to lose one of the two active X-chromosomes upon extended *in vitro* cell culture [9,10,13,23], and we recently showed that early passage female iPSCs are XaXa and become XO iPSCs upon passage (Pasque et al. unpublished). To test for X-chromosome loss in our iPSC lines, we designed a simple qPCR assay in which the X/autosome genomic DNA ratio is determined by measuring four X-linked genes (*Tfe3*, *Bcor*, *Pdha1* and *Mid1*, located on either distal region on the X-chromosome, Figure 1G, bottom) and one autosomal gene (*Gapdh)*. We found that female iPSCs at late passage were consistently losing one of the two X-chromosomes, and termed these cells XO iPSCs (Figure 1G). These results were in agreement with an independent assay using RNA *in situ*-hybridization for X-linked gene *Tsix* (Figure S1C/D and [30]). Notably, the sex-specific differences in growth (Figure 1H), in pluripotency-associated gene expression (Figures 1D/E) and pluripotency exit (Figure 1F) all correlated with the presence of two active X-chromosomes. Collectively, these results indicate that sex-specific differences in growth rates, transcription and pluripotency exit are induced in iPSCs as a result of X-chromosome reactivation in female iPSCs, but are lost upon passage concomitant with X-chromosome loss in female iPSCs.

What might be the functional relevance of sex-specific differences in cell growth? Female mouse and human embryos show a delay in post-implantation development that has been attributed to the presence of two X-chromosomes in female cells [28]. It has been suggested that the presence of two X-chromosomes slows down development to ensure that cells progress through X-chromosome inactivation [11]. We sought to test, *in vitro*, the hypothesis that reduced X-chromosome dosage provides a competitive growth advantage to cells that have undergone X-chromosome inactivation. We mixed XX ESCs and GFP-labelled XY ESCs in different ratios and followed the proportion of labeled cells over time. We found that the increased cell growth of male ESCs can provide a small advantage over a 8 day period (Figure S1K). We conclude that female mouse PSCs with two active X-chromosome recapitulate the growth delay of the early postimplantation female mammalian embryo.

Eras, Dkc1, Otud6a, Fhl1, Zfp185 and *Scml2* Dosage Do Not Explain Sex-Specific Differences in Pluripotency Exit

We sought to find the X-linked regulators that drive stabilization of pluripotency in female PSCs. We analyzed RNA sequencing (RNA-seq) and published proteomics data of male and female ESCs [13]. We selected X-linked candidate factors based on increased expression in female ESCs, and evidence that the genes are subject to X-chromosome inactivation (Tables S1/S2). We selected the candidate genes *Eras, Dkc1, Otud6a, Fhl1, Zfp185* and *Scml2* and overexpressed their cDNAs in male iPSCs (Figures S2A/B). To test the effect of overexpression on pluripotency exit, we induced differentiation by LIF withdrawal and measured pluripotency gene expression at 24h and 48h. We found that overexpression of *Eras, Dkc1, Otud6a, Fhl1, Zfp185* or *Scml2* was not sufficient to induce a delay in pluripotency exit (Figures S2C-J). Collectively, these findings do not support a significant role for these X-linked pluripotency genes in stabilizing pluripotency in female ESCs.

The Open Chromatin Landscape of ESCs Exhibits Sex-Specific Differences

To identify additional candidate regulators and to assess how X-chromosome dosage differentially primes mouse PSCs for rapid exit from pluripotency, we set out to globally define the chromatin accessibility landscape of male and female PSCs. We employed Assay for Transposase-Accessible Chromatin sequencing (ATAC-seq), a method that allows genome-wide mapping of open chromatin with high resolution [31]. We analyzed ATAC-seq datasets previously generated from male and female ESCs [32], allowing to define the open chromatin regions and the enrichment for transcription factor (TF) binding motifs associated with male and female open chromatin landscapes (Figure 2, Table S3). We first assessed differential accessibility between female and male ESCs, and found that most open chromatin regions were shared between male and female ESCs, indicating that the open chromatin landscapes of male and female ESCs are globally similar. However, we detected thousands of chromatin regions more accessible in female or in male ESCs (>2-fold, false discovery rate (FDR)<0.05), revealing that sex influences the open chromatin landscape of ESCs. We identified 5549 chromatin regions that are more open in female ESCs and 2921 chromatin regions that are more open in male ESCs, most of which were located on autosomes (Figure 2A, Table S3), which represents differences in global chromatin accessibility landscapes driven by sex. Most of the ATAC-seq peaks identified localized to distal genomic regions, suggesting enrichment in cis-regulatory sequences (Figure S3A). These results indicate that the chromatin landscape of female and male ESCs is globally similar, and also contains differentially accessible chromatin at thousands of specific genomic regions.

For chromatin regions more open in XX ESCs (defined as “XXgain”), gene ontology (GO) analysis of associated genes identified 'stem cell maintenance' as the top term (Figure 2B), and associated with multiple pluripotency-related genes (*Prdm14, Nanog, Tcl1, Esrrb*, *Dppa4, Dppa5a,* and *Pou5f1*) (Figure 2C). We identified, in our RNA-seq data, 222 differentially expressed genes (DEGs) between male and female ESCs associated with XXgain chromatin regions, most of which (174/222, 78%) were upregulated in female ESCs (including pluripotency-associated genes *Prdm14* and *Nanog*) (Figures 2C/D, Table S4/S5), likely corresponding to the stabilization of pluripotency in female ESCs [11]. Confirming these findings, increased chromatin accessibility also associated with 129 proteins that are upregulated in female ESCs, including PRDM14, NANOG, TCL1 and DPPA5A (Figure S2B, Table S5) [13]. These results indicate that the open chromatin landscape of ESCs reflects specific cellular states, where female-specific open chromatin could dictate stabilization of pluripotency in female ESCs.

In contrast to chromatin more open in female ESCs, GO analysis identified 'chordate embryonic development' as the top biological process term associated with chromatin that is more accessible in male ESCs (defined as “XYgain”) (Figure 2B). XYgain chromatin regions were associated with multiple genes involved in embryonic development, regionalization and morphogenesis (several *Hoxb* genes, *Pax3*, *Pax6*, *Fgf8, T, Krt8, Krt18, Meox1, Sox11*), several of which are not yet highly expressed in male ESCs but poised for latter activation during lineage specification (Figures 2E/F, Table S4) [33,34]. These results suggest that open chromatin associated with these lineage specification genes could poise chromatin for more

rapid transcriptional activation during differentiation of male ESCs compared with females ESCs. In further support of this, the primary ectodermal gene *Pax6* was upregulated more rapidly during differentiation of male ESCs (Figure S2D). Chromatin more accessible in male ESCs than in female ESCs also associated with 136 DEGs, 47% of which (64/136) were upregulated in male ESCs (*Krt8, Krt18, Sox11*) (Figures 2E/F, Table S4), and 53% of which were downregulated in male ESCs (Figure 2D, Table S4). In summary, these findings indicate chromatin more open in male or in female ESCs are associated with several lineage specification/differentiation related genes and multiple pluripotency genes, respectively. The chromatin accessibility landscape of male ESCs appears to prime these cells to initiate exit from pluripotency more rapidly than in female ESCs.

Motif Analysis Reveals Regulators of Sex-Specific Cell States

To gain insights in the regulatory networks that drive sex differences in ESCs, we searched for TF motifs enriched in the chromatin regions that are more open in female or in male ESCs. Motif enrichment analysis of the chromatin regions more open in female ESCs revealed a strong enrichment for the binding motif of TFs such as KLF5 (61.52%), KLF4 (27.49%), ESRRB (35.33%), SOX3 (58.44%), OCT4-SOX2-TCF-NANOG (13.18%), SOX2 (37.59%) and ZIC3 (24%) (Figures 3A/B). KLF5, KLF4, KLF2, ESRRB and SOX2 have been functionally implicated in ESC self-renewal, reviewed in [35]. OCT4 is the paramount pluripotency factor[36,37] and its co-binding with SOX2 to Oct/Sox elements [38–40] stabilizes pluripotency [41]. ZIC3 is required to maintain pluripotency [42]. Interestingly, the pluripotency-associated factor *Zic3* is located on the X-chromosome (Figure 3A), raising the possibility that ZIC3 dosage could drive X-linked driven stabilization of pluripotency in female ESCs. In summary, all top TF motifs enriched in chromatin with increased accessibility in female ESCs belong to pluripotency-associated factors, suggesting that the identified pluripotency-associated TFs participate in stabilizing the pluripotency transcriptional regulatory network of female ESCs.

By contrast, pluripotency-associated TF motifs were absent from the top motifs enriched in chromatin with increased accessibility in male ESCs (Figure 3C). Instead, within chromatin more open in male ESCs, motif enrichment analysis revealed binding sites of TFs such as JUN/AP-1 (18.99%), TEAD (32.78%), FRA2 (26.18%) and BACH2 (12.38%) (Figures 3B/C). JUN/AP-1 is a transcriptional activator complex involved in regulating many processes [43,44] including cell growth and differentiation in response to a variety of stimuli including the MAPK pathway [45,46]. TEAD is a transcriptional cofactor family involved in cell growth and proliferation via the *Hippo* signaling pathway, and TEAD2 has been shown to be required for ESC self-renewal [47,48]. FRA2 is a member of the AP-1 complex [43]. BACH2 is a hematopoietic-, neuron-specific transcriptional repressor with the potential to regulate the lineage commitment [49–52]. Additionally, male ESCs had significantly higher transcript level of *Bach2* than female ESCs (Table S1). As expected, open chromatin regions that are common between male and female ESCs still both showed enrichment of pluripotency-related TFs (not shown). We conclude that the differential enrichment of TF binding sites in sex-specific open chromatin regions provides a molecular link between transcriptional regulators, stabilization of pluripotency in female ESCs and rapid exit from pluripotency in male ESCs.

In order to identify the putative target genes, we searched for genes associated with open chromatin regions enriched for specific motifs, then determined the target genes shared for open chromatin containing more than one motif. We found that 574 genes were associated with binding motifs for all three motifs KLF, ESRRB and SOX2 (Figure 3D). These genes contained *Prdm14*. Thus, upregulation of *Prdm14* mRNA in female ESCs is associated with increased chromatin accessibility at genomic regions that contain multiple pluripotency-associated TF motifs. We sought to carry out a similar analysis for chromatin more open in male ESCs and identified 213 genes associated with both JUN/AP-1 and TEAD motifs. These genes included the early ectodermal gene *Krt18* and essential neurogenesis related gene *Sox11*, which were more expressed in male ESCs than in female ESCs. Taken together, these analyses allowed the identification of TFs that regulate a large number of cis-regulatory regions, thereby improving our understanding on how sex can drive two distinct pluripotent stem cell states.

Zic3 Dosage Does Not Modulate Sex-Specific Differences in Transcription and Pluripotency Exit

We sought to test if X-linked pluripotency-associated genes with enriched motifs identified in the open chromatin landscape of female ESCs stabilize pluripotency in female PSCs. Our motif discovery analysis identified the X-linked gene *Zic3* within the top motifs enriched in chromatin more open in XX ESCs (Figure 3A). Western blot analysis showed that female iPSCs and ESCs express higher ZIC3 protein than male iPSCs and ESCs (Figure 4A). Moreover, *Zic3* was reported to prevent endodermal lineage specification and to act as a transcriptional activator of *Nanog* expression [42,53], further suggesting that it could have a role in stabilization of naive pluripotency in female ESCs. To test the hypothesis that increased *Zic3* dosage stabilizes pluripotency in female ESCs, we generated *Zic3* heterozygous deletions to reduce *Zic3* dosage in female ESCs (Figures 4B/C, S4A/B). However, *Zic3*+/- female ESCs maintained female-like expression of *Prdm14*, *Nanog* and *Tcl1* and also displayed delayed exit from pluripotency (Figure 4D). Overexpression of *Zic3* in male iPSCs also maintained male-like pluripotency gene expression and differentiation kinetics (Figures S4C/D). Since reducing or increasing *Zic3* dosage in ESCs does not modulate pluripotency-associated gene expression or pluripotency exit, *Zic3* dosage does not explain the sex-specific differences in pluripotency-associated gene expression and pluripotency stabilization.

Heterozygous *Dusp9* Deletion in Female ESCs Induces Male-like DNA Methylation and Maintains Female-like Pluripotency Exit

X-chromosome dosage has been shown to modulate the DNA methylation landscape of ESCs through the X-linked MAPK phosphatase *Dusp9 [13]*. Reducing DUSP9 dosage in female ESCs rescues global DNA hypomethylation by inducing male-like global DNA methylation levels[13]. However, whether *Dusp9* heterozygous deletion induces a male-like transcriptome, pluripotency exit and growth required additional experiments. We set out to investigate whether *Dusp9* heterozygous deletion and its associated DNA methylation level affect the sex-specific transcriptional state and pluripotency exit of female ESCs. We generated *Dusp9* heterozygous deletions in female XX ESCs using CRISPR-Cas9 genome editing, resulting in two independent *Dusp9*+/- XX ESC clones (Figures 5A/B, Figures S5A/B). *Dusp9*+/- ESCs maintained two active

X-chromosomes (Figures S5C/D) since we used polymorphic ESCs less susceptible to X-chromosome loss [13,54]. To determine if *Dusp9*+/- ESCs acquire male-like transcription, we analyzed the transcriptome of *Dusp9*+/- ESCs, *Dusp9*+/+ ESCs and *Dusp9*+ (XY) ESCs using RNA-seq. Principal component analysis (PCA) placed *Dusp9*+/- ESCs closer to *Dusp9*+/+ ESCs but further away from XY ESCs (Figure 5C). We corroborated this finding using unsupervised clustering of the most variable genes between all 4 cell types, where *Dusp9*+/- ESCs clustered together with *Dusp9*+/+ ESCs, and away from XY ESCs (Figure 5D). These results demonstrate that, surprisingly, reducing *Dusp9* dosage in female ESCs is not sufficient to induce a male-like transcriptome, unlike DNA methylation.

DEG analysis identified 948 DEGs between *Dusp9*+/- ESCs and control *Dusp9*+/+ ESCs (DEGs between *Dusp9*+/- ESCs and *Dusp9*+/+ ESCs shared between two independent *Dusp9*+/- ESC clones, Figures 5E, S5E, Table S6). GO analysis revealed the PI3K-Akt and MAPK pathways among the top pathways enriched in DEGs (Figure 5E). Unsupervised clustering analysis showed the activation of most MAPK target genes, in agreement with the function of *Dusp9* as a MAPK inhibitor (Figure 5F) [55]. Although the upregulation of MAPK target genes was expected, the striking difference of *Dusp9*+/- ESCs with XY ESCs was surprising because XY ESCs, like *Dusp9*+/- ESCs, also have a single active copy of *Dusp9*. These results suggest that there may be other X-linked genes participating in the regulation of MAPK signaling and that reducing *Dups9* dosage in female ESCs also modulates Akt target genes.

Surprisingly, in *Dusp9*+/- ESCs, we detected a clear upregulation of *Xist* and *Jpx* and a downregulation of *Tsix*, suggesting that *Dusp9* dosage may, at least partially, influence the X-chromosome inactivation center in female ESCs (Figure S5F). X-chromosome inactivation is controlled by the X-chromosome inactivation center containing key regulatory elements and long non-coding RNAs such as the X-chromosome inactivation initiator *Xist* and the *Xist* antagonist *Tsix* as well as other long noncoding RNAs such as *Jpx* (reviewed in [56]). The upregulation of *Xist* in *Dusp9*+/- ESCs did not lead to *Xist* cloud formation (Figure S5C).

To study the effects of *Dusp9* heterozygous deletion in female ESCs on pluripotency exit, we subjected *Dusp9*+/- ESCs, *Dusp9*+/+ ESCs and XY ESCs to LIF withdrawal differentiation for 24h followed by RNA-seq analysis. Both PCA and unsupervised hierarchical clustering based on the top 500 or 200 most variable genes, grouped *Dusp9*+/- ESCs together with the parental *Dusp9*+/+ ESCs, separately from XY ESCs (Figures 5C, 5G, S5G), therefore reducing *Dusp9* dosage is not sufficient to induce male-like pluripotency exit. In agreement with this finding, most delayed pluripotency-associated genes in *Dusp9*+/+ ESCs still showed a delay in pluripotency exit in *Dusp9*+/- ESCs (29/42 genes, 70%), including genes such as *Prdm14* and *Nanog* which maintained a female-like pattern in *Dusp9*+/- ESCs during pluripotency exit (Figure 5H, Table S7). We validated the expression of *Prdm14* and *Nanog* using RT-qPCR analyses (Figure 5I). Hence, we conclude that reducing the dosage of *Dusp9* in female ESCs is not sufficient to induce a male-like transcriptome or accelerate pluripotency exit to a male-like state, despite changes in the expression level of multiple genes in MAPK and Akt signaling pathways. However, our *Dusp9*+/- ESCs did show male-like global DNA methylation (Figure S5H), corroborating recent findings [13]. In addition, we show that *Dusp9* overexpression in male ESCs was not sufficient to induce a female-like delay in differentiation (Figures S5I-L)

despite inducing female-like global DNA hypomethylation [13], consistent with a previous report [11]. Interestingly, we found that *Dusp9*+/- ESCs grew as slow as the parental *Dusp9*+/+ ESCs, both slower than XY ESCs (Figure 5J), therefore reducing *Dusp9* dosage is not sufficient to induce male-like cell growth. This result suggests that there maybe other X-linked genes regulating sex-specific growth in PSCs. Altogether, these results indicate that reducing *Dusp9* dosage in female ESCs does not appear to be sufficient to induce male-like transcription and pluripotency exit, in contrast to the acquisition of male-like DNA methylation. Hence, heterozygous *Dusp9* deletion molecularly uncouples global DNA methylation from the pluripotency exit delay of female ESCs.

DISCUSSION

Induction of naive pluripotency during reprogramming to iPSCs and during *in vivo* development in inner cell mass (ICM) leads to X-chromosome reactivation in murine female cells [17–19,57]. The consequences of X-chromosome dosage imbalance between female (XX) and male (XY) cells on mouse iPSCs remained unclear until now. In addition, the regulatory mechanisms at the basis of distinct sex-specific features in mouse PSCs were incompletely understood. In this study, we addressed these questions by analyzing the growth properties, transcriptional states and pluripotency exit of isogenic male and female iPSCs. We identified sex and X-chromosome dosage as important factors influencing the molecular and functional properties of iPSCs. By employing epigenomic analyses we found that sex modulates the open chromatin landscape of ESCs. Moreover, using genome editing we found that sex-specific differences in pluripotency exit and cell growth can be molecularly uncoupled from DNA methylation.

Impact of Sex and X-chromosome Dosage on Growth, Transcription and Pluripotency Exit

One outcome of our study is that the number of active X-chromosomes correlates with sex-specific differences in growth, transcription and pluripotency exit in iPS cells (Figure 1), in addition to differences in DNA methylation [22]. Reprogramming somatic cells to iPSCs is an important system to study erasure of epigenetic memory and pluripotency. Sex does not appear to influence the efficiency of iPSCs generation, since we previously showed that male and female cells reprogram with similar efficiencies in this system [30]. However, we have now established that the presence of two active X-chromosomes as a result of reprogramming to pluripotency in female cells is associated with slower growth in iPSCs, increased pluripotency-associated gene expression, and delayed pluripotency exit. These differences are likely caused by changes in X-chromosome dosage, consistent with previous discoveries in mouse ESCs [6,9,11,14], in human ESCs [7,8,58] and in postimplantation mammalian embryos [6,28,59]. The notion that X-chromosome dosage influences the molecular and functional properties of iPSCs [6,11,22] is further supported by the loss of sex-specific differences concomitant with loss of one X-chromosome in female iPSCs, in agreement with previous observations in ESCs [9,11,13,14] and in iPSCs. The important point is that studies of reprogramming to iPSCs should consider

the number of active X-chromosomes as a modulator of the transcriptional and growth states of iPSCs and cells of different sex should always be studied separately, but also often both considered.

The presence of two X-chromosomes has been associated with delayed embryo post-implantation growth in several mammalian species [28,59]. Here we show for the first time that this property is recapitulated in mouse ESCs and iPSCs, where XX ESCs grow slightly, and significantly slower than XY and XO ESCs (Figure 1). Since the growth differences are maintained after dual GSK3B and ERK inhibition, additional pathways are likely involved. One hypothesis is that there could be a competitive growth advantage of cells that have undergone X-chromosome inactivation in the post-implantation mammalian embryo to select against remaining cells with two active X-chromosomes that fail to undergo X-chromosome inactivation. Our *in vitro* experiment suggests that X-chromosome inactivation could indeed provide a small growth advantage. However, this hypothesis remains to be tested *in vivo*.

Impact of *Dusp9* Dosage on Pluripotent States

A previous study showed that *Dusp9* modulates DNA hypomethylation in female mouse ESCs [13]. However, the effects of reducing *Dusp9* dosage in XX ESCs on growth, transcription and pluripotency exit were unknown. An important outcome of our analyses is that female *Dusp9* heterozygous XX ESCs display male-like global DNA methylation levels and maintain female-like growth and delayed pluripotency exit (Figure 5). Thus, we propose that global DNA hypomethylation can be molecularly uncoupled from stabilization of pluripotency in XX ESCs. This result was unexpected because reducing the expression of DNMTs in male ESCs is associated, at least in part, with delayed pluripotency exit [11]. However, it was reported that the ICM of male and female embryos show comparable DNA methylation [13], despite delayed female development, suggesting that DNA hypomethylation and stabilization of pluripotency can be uncoupled both *in vivo* and *in vitro*. Our results therefore suggest that sex-specific DNA methylation levels and stabilization of pluripotency in PSCs are regulated, at least in part, by distinct X-linked genes (*Dusp9* for DNA methylation levels, other gene(s) for delayed pluripotency exit and growth). Our results do not support a major role of several X-linked genes, including *Zic3, Dkc1, Otud6a, Fhl1, Zfp185*, *Scml2* and *Eras* in stabilizing pluripotency. Therefore, identifying the X-linked gene(s) responsible for delayed pluripotency exit and slower growth of female mouse PSCs warrant future studies [6]. An interesting candidate is the recently-identified X-linked transient octamer binding factor 1 (TOBF1) [60], since it was shown to sustain pluripotency. It is also possible that other regulators of the Erk pathway are involved. A previous study in human ESCs reported that human primed PSCs with eroded X-chromosome inactivation and increased expression of the MAPK/ERK downstream effector ELK-1 have decreased expression of TRA-1-60, a marker of the differentiated state [8]. However, human primed PSCs studies are likely not compatible with mouse naive PSCs studies because they reside in distinct pluripotent states. In addition, there has been conflicting reports on the effects of *Dusp9* overexpression on ERK phosphorylation in mouse ESCs, despite the expected transcriptional inhibition of ERK targets genes [6]. One study found that *Dusp9* promotes phosphorylated ERK (pERK) [13], while another found reduced pERK after *Dusp9*

overexpression [55]. Our results are more in agreement with the latter study [13] since, unexpectedly, *Dusp9* heterozygous deletion appeared to decreased pERK levels, concomitant with a high increase in expression of many ERK target gene. Identifying additional X-linked regulators of sex-specific differences, including ERK regulators, deserves future investigations.

Differences in the Chromatin Landscape Underlie Sex-Specific Pluripotency States

To better understand what drives sex-specific features of the pluripotent regulatory network in ESCs, we explored the open chromatin landscapes of male and female ESCs. While both male and female ESCs possessed similar open chromatin landscapes, thousands of chromatin regions were differentially accessible in male and female ESCs (Figure 2). These differentially accessible regions could underlie the distinct transcriptional regulatory networks of male and female ESCs. Decoding differentially accessible chromatin regions, we identified several pluripotency genes such as *Prdm14*, *Tcl1* and *Nanog* with increased accessibility in female ESCs. These genes have been associated with naive pluripotency hence they could act as targets to stabilize naive pluripotency in female ESCs [11]. We went further by identifying a catalogue of cis-regulatory regions including promoters that are modulated by sex in ESCs. These observations indicate that X-chromosome dosage modulates the chromatin accessibility landscapes of ESCs.

Unexpectedly, chromatin regions more open in female ESCs associated with several terms related to trophectoderm and placenta development (Figure 2B). Male mouse ESCs do not readily differentiate into trophectoderm [61]. However, male *Dnmt1* knockout ESCs, which show reduced global DNA methylation like female ESCs [9–11,62], have been shown to reacquire trophectoderm differentiation potential in addition to embryonic lineage differentiation capacity [9–11,62]. Collectively, these observations raise the possibility that female ESCs may reacquire trophectoderm differentiation potential due to global DNA hypomethylation. Therefore, female ESCs may not only be stabilized in naive pluripotency, but they may also unlock an extra-embryonic differentiation program as a result of global DNA hypomethylation, highlighted here by the acquisition of chromatin accessibility related to trophectoderm differentiation. Nevertheless, global DNA hypomethylation in female ESCs also leads to imprint erasure, which was suggested to compromise development [14,15,63]. Our results suggest that female ESCs grown in S/L may acquire extended pluripotent stem cell properties characterized by both trophectoderm and embryonic lineage differentiation capacity, in addition to loss of imprints. This hypothesis can be tested by subjecting female ESCs to trophectoderm differentiation assays.

Transcriptional Regulators of Sex-Specific Pluripotent Stem Cell States

Decoding differentially accessible chromatin allowed us to distinguish distinct sets of enriched TF binding motifs in male and female ESCs. Specifically, we identified motifs for KLF5, ESRRB, SOX3, OCT4-SOX2-TCL-NANOG, SOX2 and ZIC3 enriched in chromatin more open in female ESCs, all of which have been implicated in pluripotency [35–37,41,42]. These results suggest that the stabilization of pluripotency in female ESCs is mediated by these core master regulators. However, *Zic3* heterozygous deletion had no effect on stabilization of pluripotency.

Although no TF ChIP-seq data is available for female ESCs to date, our in silico analyses identified a high confidence set of direct putative KLF5, ESRRB, SOX2 and OCT4 targets in female ESCs, including known pluripotency genes. Moreover, the specific enhancer associated with *Prdm14* which becomes more accessible in female ESCs overlaps with ChIP-seq binding sites of OCT4, SOX2 and NANOG in male ESCs (not shown), further suggesting that the binding of master pluripotency regulators takes place at these more accessible regions in female ESCs. Our results raise the possibility that pluripotency is stabilized in female ESCs by binding of core pluripotency factors to a subset of sex-specific regulatory elements that include *Prdm14*, *Tcl1* and *Nanog*. Dual promotion of *Prdm14* and *Nanog* expression represents a possible naive pluripotency stabilization mechanism consistent with their established functions in ESCs [64,65].

In contrast to the female state, differentially accessible chromatin more open in male ESCs identified AP-1 and TEAD as candidate regulators, which have not been implicated in sex-specific regulation of pluripotency before. JUN/AP-1 control many cellular processes including proliferation, apoptosis and differentiation in response to a variety of stimuli including the MAPK pathway (reviewed in [43]). TEAD is a TF family involved in cell growth and differentiation via the Hippo singaling pathway (reviewed in [66] and [47]). The role of AP-1/TEAD TFs in the context of sex-specific transcription in ESCs warrants future studies.

To conclude, this is the first report which reveals that DNA hypomethylation and delayed pluripotency exit can be uncoupled in female mouse ESCs. Furthermore, our study shows for the first time that sex-specific differences in cell growth, transcription, and pluripotency exit in iPSCs correlate with the number of active X-chromosomes. Using information from the genome, the epigenome and the transcriptome we gained insights into modulation of the open chromatin landscape and the transcriptional regulatory network of ESCs by sex. Furthermore, better understanding how sex modulates pluripotency of iPSCs will have important implications for disease modeling and regenerative medicine. Our results raise the possibility that the pluripotent state can be harnessed for sex-specific regenerative medicine.

EXPERIMENTAL PROCEDURES

Mice and reprogramming

MEFs were isolated from individual E14.5 mouse embryos obtained from a cross between wild type (WT) C57BL/6 and homozygous Rosa26:M2rtTA, TetO-OSKM mice [26]. Individual embryos were genotyped for sex using *Ube1* as previously described (See Table S8 for primer sequence) [30] using homemade Taq DNA Polymerase and grown in MEF medium [DMEM (Gibco, 41966-052) supplemented with 10% (v/v) fetal bovine serum (FBS, Gibco, 10270-106), 1% (v/v) penicillin/streptomycin (P/S, Gibco, 15140-122), 1% (v/v) GlutaMAX (Gibco, 35050-061), 1% (v/v) non-essential amino acids (NEAA, Gibco, 11140-050), and 0.8% (v/v) beta-mercaptoethanol (Sigma, M7522)]. Reprogramming was induced by doxycycline (final 2 µg/ml) in mouse ESC medium [KnockOut DMEM (Gibco, 10829-018) supplemented with 15% FBS, 1% (v/v) P/S, 1% (v/v) GlutaMAX, 1% (v/v) NEAA, 0.8% (v/v) beta-mercaptoethanol, and mouse

LIF] in the presence of ascorbic acid (final 50 µg/ml). Individual colonies were picked at day 16 onto irradiated male feeders in ESC medium without doxycycline or ascorbic acid and expanded for three passages, eventually obtaining 10 female iPSC lines (lines 1, 4, 5, 6, 8, 12, 13, 14, 16, 17, 18) and 11 male iPSC lines (lines 19, 20, 21, 22, 23, 24, 25, 26, 27, 28, 29) at passage (P) 4 (Figure S1B). iPSC lines 1, 4, 8, 12, 14, 16, 20, 21, 22, 24, 26 and 28 were also used in another study (Pasque et al. unpublished). All animal work carried out in this study is covered by a project license approved by the KU Leuven Animal Ethics Committee.

Cell lines and culture

XY ESCs (V6.5) and XX ESCs (F1-2-1) were obtained from the Plath laboratory. Independently-derived XY ESCs and XX Mus/Cas ESCs were also used here and obtained from the Deng laboratory [25]. GFP-labelled (Oct4-GiP) XY ESCs were previously described [67]. ESCs and iPSCs (male iPSC line 4, 8, 16; female iPSC line 20, 21, 22) were expanded on top of male WT feeders in mouse ESC medium (S/L condition), eventually early passage cells (iPSCs: P6-P8) and late passage cells (iPSCs: P13-P14) were used for further experiments. ESCs and iPSCs (male iPSC lines 1, 4, 8, 12, 16; female iPSC lines 19, 20, 21, 22, 23, 26) were adapted to 2i/LIF, where cells grown on feeders in S/L condition (iPSCs: P4) were switched to new tissue culture dishes precoated with gelatin (from porcine skin, 0.1% g/v final, Sigma, G2500) without feeders in 2i/LIF medium [N2B27 basal medium (Neurobasal medium (50% v/v final, Gibco, 21103-049) and DMEM/F-12 medium (50% final, Gibco, 11320-074) supplemented with L-Glutamine (1.25 mM final, Gibco, 25030081), NDiff Neuro2 supplement (1x final, Millipore, SCM012), B27 supplement (1x final, Gibco, 17504-044), 0.8% (v/v) beta mercapto ethanol, and 1% (v/v) P/S) supplemented with 0.35% (g/v) Bovine Serum Albumin (BSA, Sigma, A7979), homemade mouse LIF, GSK3 inhibitor CHIR-99021 (3 µM final, Axon Medchem, Axon 1386) and MEK inhibitor PD0325901 (1 µM final, Axon Medchem, Axon 1408)] for four passages.

Plasmids Constructs

The full-length mouse cDNAs of *Dusp9*, *Zic3*, *Eras*, *Dkc1, Otud6a, Fhl1, Zfp185*, and *Luciferase* (from pGL2-Basic Promage, E1641), *NLS-cherry* was cloned into pENTR vectors (Invitrogen, K240020) with either a C-terminal or a N-terminal HA tag, or no tag, and recombined into pPB-CAG-Dest-pA-pgk-bsd (PB-DEST-BSD) destination vectors. The PB-Scml2-BSD plasmid was obtained by recombining the pDONR221-Scml2 plasmid [68] into PB-DEST-BSD. Guide RNAs (gRNAs) were cloned into SapI digested pZB-sg3 [69]. All gRNAs sequences are included in Table S8, Figures S4A, S5A. All constructs were verified by DNA Sanger sequencing.

Generation of stable male iPSCs overexpressing X-linked candidate genes

Male iPSCs (line 4, P5, grown on feeders in S/L conditions) were feeder-depleted before seeding in six-well plates precoated with 0.1% gelatin in S/L medium at a density of 650,000 cells per well, which were co-transfected with 1 ug of PB expression constructs encoding candidate genes and 3 ug of pCAGP Base [70] using 10 µl Lipofectamine 2000 (Invitrogen, 11668027). Transfected cells were selected with 20 µg/mL blasticidin (Fisher BioReagents, BP2647100) supplemented to the medium for two days starting from 24h after transfection and maintained with 5 µg/mL blasticidin thereafter.

Generation of female XX ESC lines with *Dusp9* or *Zic3* heterozygous deletions

2000,000 female F1-2-1 ESCs (P19, grown on feeders in S/L condition) were resuspended in 1 ml of S/L medium and co-transfected with 2 ug of a plasmid expressing Cas9 under a CAG promoter and 1 ug of 2 plasmids (pZB-sg3 [69]) containing gRNAs (Table S8) using 10 µl Lipofectamine 2000 (Invitrogen, 11668027) (Figures S4A, S5A) for one hour before plating on 4-drug resistant (DR4) feeders. Transfected cells were selected with 2 µg/mL puromycin (Fisher BioReagents, BP2647100) on DR4 feeders in ESC medium for two days starting from 24h after transfection, and expanded at low density on WT feeders in 10cm dishes. Individual colonies were picked onto WT feeders, expanded for another two passages and genotyped for both WT and mutant alleles (primers in Table S8). WT and mutant alleles were further verified by DNA Sanger sequencing.

Differentiation

To induce differentiation towards epiblast-like cells (EpiLCs), ESCs and iPSCs (male lines: 1, 4, 8, 12, 16; female lines: 19, 20, 21, 22, 23, 26), which had been adapted to 2i/LIF conditions, were plated in N2B27 basal medium supplemented with 10 ng/ml Fibroblast Growth Factor-basic (Fgf2, Peprotech, 100-18C) and 20 ng/ml Activin A (ActA, Peprotech, 120-14E) on Fibronectin (5 ug/10 cm^2, Millipore, FC010-5MG)-coated tissue culture plates at a cell density of $8*10^4$ cells/cm^2 for four days, during which medium was refreshed daily and cells were harvested at different time points (0h, 12h, 1 day, 2 days, 3 days and 4 days), as previously described [11]. ESCs (WT female and male ESCs, *Dusp9*+/- ESCs, and *Zic3*+/- ESCs) and iPSCs (male iPSC lines 4, 8, 16; female iPSC lines 20, 21, 22; both early and late passages) grown in S/L condition were differentiated in the absence of feeders by LIF withdrawal (similar as mouse ESC medium but with 10% FBS and without LIF) at a cell density of $4*10^4$ cells/cm^2 for two days, during which medium was refreshed daily and cells were harvested at different time points (0h, 24h and 48h), as previously described [11]. Likewise, male iPSC lines overexpressing X-linked genes were differentiated by LIF withdrawal with 5 µg/mL blasticidin in the absence of feeders.

Cell growth assay

ESCs and iPSCs were plated in 24-well plates at a cell density of $4*10^4$ cells/cm^2 for two days, during which medium was refreshed daily and cells were counted at different time points (0h, 12h, 24h, 36h and 48h). The cell numbers are presented as fold changes relative to cell numbers at 0h.

Immunofluorescence

Immunofluorescence analyses were carried out largely as described previously [30], using the following primary antibodies: NANOG (eBioscience, 14-5761 clone eBioMLC-51, 1/200; and Abcam, ab80892, 1/ 200), DPPA4 (R&D, AF3730, 1/200), HA (Cell Signaling Technology, 2367S, 1/100), DUSP9 (Abcam, ab167080, 1/100). Images were acquired using an ApoTome Zeiss Microscope equipped with an AxioCam MRc5 camera. ESC and iPSC lines were defined as NANOG+ or DPPA4+ when >50% cells showed NANOG or DPPA4 staining signal.

RNA FISH

RNA Fluorescence In Situ Hybridization (RNA FISH) analyses were carried out mostly as described previously using double stranded directly labelled DNA probe for *Tsix/Xist [30]*. Images were acquired using an ApoTome Zeiss Microscope equipped with an AxioCam MRc5 camera. Single-cell resolution analysis of *Tsix* biallelic expression in iPSCs and ESCs was determined by calculating the ratio of cells with biallelic *Tsix* expression to the cells with monoallelic or biallelic *Tsix* expression.

Genomic DNA extraction and qPCR

Genomic DNA (gDNA) was extracted from feeder-depleted ESCs and iPSCs using the PureLink Genomic DNA Kit (Invitrogen, K1820) and qPCR was performed using the Platinium SYBR Green qPCR SuperMix-UDG kit (Invitrogen, 11733046) on a ABI ViiA7 real-time PCR system (Applied Biosystems), following the manufacturer's protocol. Primers against four X-linked genes (*Tfe3, Bcor, Pdha1, and Mid1*) covering the two distal parts of the mouse X-chromosome are listed in Table S8 (Figure 1G). The standard curve was derived from serial dilutions of gDNA from XY ESCs (V6.5). All qPCR assays used had an efficiency above 95%. Relative quantities of each gene were measured as arbitrary units from comparison to the standard curve. The ratio of X-chromosome to autosome (X/Autosome Ratio) in DNA level was presented as the average ratio of the X-linked gene quantity (*Tfe3, Bcor, Pdha1* and *Mid1*) to the autosomal gene quantity (*Gapdh*), in other words X/Autosome Ratio = (*Tfe3/Gapdh* + *Bcor/Gapdh* + *Pdha1/Gapdh* + *Mid1/Gapdh*)/4 .

RT-qPCR

Total RNA was extracted using the RNeasy Mini Kit (Qiagen, 74106) or TRIzol (Invitrogen, 15596026). cDNA synthesis was performed using the SuperScript III First-Strand Synthesis SuperMix kit (Invitrogen, 11752-050) and RT-qPCR was performed using the Platinium SYBR Green qPCR SuperMix-UDG kit (Invitrogen, 11733046) and on the ABI ViiA7 real-time PCR system, following the manufacturer's protocol. Primers used are listed in Table S8. The standard curve was derived from serial dilutions of cDNA. All assays used had an efficiency above 95%. Relative quantities of each transcript were calculated as arbitrary units from comparison to the standard curve. Relative expression level of the target transcript was presented as the ratio of the target transcript quantity to the housekeeping transcript (Gapdh) quantity. Logarithm values (base 2) of relative expression levels were used for assessment of the gene expression kinetics during differentiation. The relative gene expression levels of five pluripotency-associated genes (*Prdm14, Nanog, Tcl1, Rex1* and *Esrrb*) from iPSCs (male lines: 1, 4, 8, 12, 16; female lines: 19, 20, 21, 22, 23, 26) and ESCs (V6.5 male ESCs and F1-2-1 female ESCs) at 0h and 24h of EpiLC differentiation were used for unsupervised clustering comparison, which was performed in R with heatmap.2 function in package "gplots".

RNA sequencing

Total RNA was isolated from two independent female *Dusp9*+/- ESC lines, *Dusp9*+/+ XX and XY ESCs in both the undifferentiated state and the differentiated state after 24 hours of LIF

withdrawal using TRIzol following the manufacturer's protocol. 4 µg of total RNA was used for construction of stranded poly(A) mRNA-Seq library with the KAPA stranded mRNA Library prep kit (KAPA Biosystems, KK8421). Library concentrations were quantified with the Qubit dsDNA HS (High Sensitivity) Assay Kit (Invitrogen, Q32854), and equimolar amounts were pooled for single-end sequencing on an Illumina HiSeq 4000 instrument (Illumina) to yield ~20 million (range 16-23 million) 36bp long reads per sample.

Differential gene expression analysis

Reads from all datasets (*Dusp9*+/- ESCs, *Dusp9*+/+ ESCs and XY ESCs) were aligned to mouse reference genome GRCm38/mm10 using STAR (v2.5.3a) with default parameters followed with conversion to BAM format sorted by coordinate. The mapping efficiencies of the datasets were >69% of uniquely mapped reads. Subsequently, the featureCounts function from the R Bioconductor package "Rsubread" was used to assign mapped reads to genomic features. For downstream analyses, only the genes with CPM value (count-per-million) higher than 0.5 in at least two libraries were retained. The resulting read count matrix (Table S5) was used as the input for PCA with the top 500 most variable genes. Differential gene expression analysis was performed using the edgeR quasi-likelihood pipeline in R [71]. Obtained p-values were corrected for multiple testing with the Benjamini-Hochberg method to control the FDR. DEGs were defined on the basis of both FDR < 0.05 and fold difference ≧ 1.5. Venn diagrams were generated using an online tool as previously described [72]. Heatmaps were created using unsupervised hierarchical clustering of both 200 most variable genes and the different samples and generated in R using the heatmap.2 function of the package "gplots".

Definition of pluripotency exit delay

In order to quantitatively measure the pluripotency exit delay in *Dusp9*+/+ ESCs, XY ESCs and *Dusp9*+/- ESCs, an expression matrix containing genes related to stem cell maintenance (GO0019827) and stem cell development (GO0048864) with normalized counts was created. The ratio of expression level at 24h to 0h of differentiation (24h/0h ratio) was calculated for both WT XY and *Dusp9*+/+ ESCs. Only the genes that were downregulated in XY ESCs and had 24h/0h ratios < 0.75 passed the filtering. Subsequently, 24h/0h ratios were compared between WT XX and XY ESCs, if the resulting value was >1, the gene was qualified as a "delayed" gene during the pluripotency exit in *Dusp9*+/+ ESCs. For these genes, the same algorithm was applied to evaluate the delay in *Dusp9*+/- ESCs.

Differential chromatin accessibility analysis

ATAC-seq data for mouse XX ESCs and XY ESCs were retrieved from a previous collection (accession numbers are GSM2247118 and GSM2247119 in XX and XY ESCs, respectively) [32]. Single-end-reads raw data were analyzed using the ATAC-seq pipeline from the Kundaje lab (Version 0.3.3)[73]. Briefly, the raw reads were first trimmed using cutadapt (version 1.9.1) to remove adaptor sequence at the 3′ end. The trimmed reads were aligned to reference genome (mm10) using Bowtie2 (v2.2.6) using the '--local' parameter. Single-end reads that aligned to the genome with mapping quality ≥30 were kept as usable reads (reads aligned to the

mitochondrial genome were removed) using SAMtools (v1.2). PCR duplicates were removed using Picard's MarkDuplicates (Picard v1.126). Open chromatin regions (peak regions) were called using MACS2 (v2.1.0) using the '-g 1.87e9 -p 0.01 --nomodel --shift -75 --extsize 150 -B --SPMR --keep-dup all --call-summits' parameter [74]. The differential chromatin accessibility analysis and related plots were performed using the DiffBind package using the 'summits=250, default DESeq2, log2fold=1, FDR<=0.05' parameter [75]. GO analysis for Biological Process terms was performed using GREAT (v3.0.0) analysis [76] with the mm10 reference genome, where each region was assigned to the single nearest gene within 1000kb maximum distance to the gene's TSS.

Motif Discovery Analysis

Known motif search was performed using program of findMotifsGenome.pl in the HOMER package (v4.9.1) with 'mm10 -size -250,250 -S 15 -len 6,8,10,12,16' parameters [77]. Incidences of specific motif was examined by the program of annotate-Peaks.pl in the HOMER package with size parameter ''-size 500''.

Western blots

Cells were detached from plates with 0.25% Trypsin-EDTA (Gibco, 25200056), pelleted before addition of RIPA lysis buffer (Sigma, R0278-50ML) supplemented with 1% (v/v) Protease inhibitor cocktail (Sigma, P8340-1ml) and 1% (v/v) Phosphatase inhibitor Cocktail 3 (Sigma, P0044-1ML), and lysed on ice for 30 min. The lysates were spun for 10 min at 13000 rpm. The protein concentration was determined with BCA protein assay kit (Pierce, 23225). Each sample with 15 µg of total protein was denatured in 1x LDS Sample buffer (Life Technologies, NP0007) with 100 mM DTT for 5 min at 98°C. The cell lysates were loaded onto a 4%–15% mini-Protean TGX gel (Bio-Rad #456-1083), electrophoresed, and transferred to nitrocellulose membranes (VWR,10600002). Membranes were blocked in PBS 0.1% (v/v) Tween-20 and 5% (g/v) blotting reagent (Bio-Rad, 1706404) and incubated with the following primary antibodies overnight at 4°C: rabbit anti-NANOG (Abcam, ab80892, 1/1000), rabbit anti-DUSP9 (Abcam, ab167080, 1/500), mouse anti-DKC1 (Santa Cruz, sc-365731, 1/250), mouse anti-HA (Cell Signaling Technology (CST), #2367S, 1/1000), rabbit anti-Phospho-ERK1/2 (Thr202/Tyr204) (CST, #4370, 1/2000), mouse anti-ERK1/2 (CST, #4696, 1/2000), and mouse anti-ACTIN (Abcam, ab3280, 1/5000). After extensive PBS 0.1% Tween-20 (PBS-T) washes, membranes were incubated with a secondary HRP-conjugated goat anti-mouse IgG antibody (Bio-Rad, 1706516, 1/5000) or goat anti-rabbit IgG antibody (Bio-Rad, 1706515 1/5000) for 30 minutes at room temperature. After another round of extensive PBS-T washes, protein expression was visualized using the ECL chemiluminescence reagent (Perkin-Elmer, NEL103001EA) and LAS-3000 imaging system (Fuji). Data were analyzed with ImageJ.

Statistical analysis

Statistical tests were performed using the Graphpad Prism 5 software (GraphPad Software). Unpaired two-tailed t-test, one-way ANOVA with Dunnett's multiple comparisons test or two-way repeated-measures ANOVA were used as indicated. All data are presented as the mean±SEM. p-values <0.05 were considered statistically significant.

Data Availability

The ATAC-seq data discussed in this publication have been deposited in NCBI's Gene Expression Omnibus (Edgar et al., 2002) and are accessible through GEO Series accession number GSM2247118 and GSM2247119. The GEO accession number for the RNA-seq data reported in this paper is GSE110215.

ACKNOWLEDGEMENTS

We apologize to the authors that we could not cite due to space constraint. We thank to Edda Schulz, Frederic Lluis Vinas and Stein Aerts for discussions; Rudolf Jaenisch for providing mice; Qiaolin Deng for the Mus/Cas ESCs, Ye-Guang Chen for the *Dusp9* plasmids, Miguel Branco for the Scml2 plasmids, José Silva for the PiggyBac plasmid, Mitchell Guttman and Jesse Engreitz for the pZB-sg3 plasmid, Sein Aerts, Liesbeth Minnoye, Kristofer Davie and Xinlong Luo for help with bioinformatics and ATAC-seq; Kenjiro Shirane and Hiroyuki Sasaki for providing processed data. We thank Edda Schulz, Kathrin Plath, Constantinos Chronis and Kian Koh for critically reading the manuscript. We are grateful to the help of KU Leuven FACS Core, Genomics Core and Mouse facility, Metabolomics Core, VIB/KU Leuven and SCIL. This work was supported by The Research Foundation – Flanders (FWO) (Odysseus Return Grant G0F7716N to V.P.), the KU Leuven Research Fund (BOFZAP starting grant StG/15/021BF to V.P., C1 grant C14/16/077 to V.P. and Project financing), and FWO Ph.D. fellowships to A.J. (1158318N).

AUTHOR CONTRIBUTIONS

Conception and design, J.S. and V.P.; Experiments, J.S., N.D.G., L.V., T.O., I.T. and V.P.; Analyses, J.S; RNA-seq analyses, A.J. and J.S.; Writing V.P. and J.S. with input from all authors; Supervision, V.P.

FIGURE LEGENDS

Figure 1. Sex-specific differences in transcriptional, pluripotency exit and cell growth in mouse iPSCs.

(A) Scheme of female and male iPSCs derivation, characterization and differentiation.
(B) Representative images of female and male iPSCs and ESCs grown on feeders in S/L condition.
(C) Growth curves and doubling times of female and male iPSCs (i) and ESCs (ii) in S/L condition. Cell were counted at the indicated time points and presented as fold changes relative to averages (±SEM) of male and female iPSC lines at 0h (three lines each, n=1, left panel) in early passage (P6) and of male and female ESCs (one line each, n=3, right panel), respectively. Growth curve: *p<0.05, ***p<0.001, Male iPSCs vs Female iPSCs, Male ESCs vs Female ESCs, two-way repeated-measures ANOVA with Bonferroni posttests. Doubling time (Td): *p<0.05, **p<0.01, Male iPSCs vs Female iPSCs, Male ESCs vs Female ESCs, unpaired two-tailed t-test.

(D) RT-qPCR analysis for pluripotency-associated gene expression in iPSCs grown in S/L in both early and late passages. The expression values are represented as averages (±SEM) of male and female iPSC lines (three different lines each) in early passage (P8) and late passage (P14), respectively. Statistical significance was analysed using the unpaired, two-tailed t-test (**p<0.01).
(E) Western blot analysis for NANOG, DNMT3B and DUSP9 protein in iPSCs grown in S/L in both early and late passages. Lower panel: quantification using ACTIN as a loading control. The protein values are represented as averages (±SEM) of male and female iPSC lines (n=3 lines each) in early passage (P6) and late passage (P13), respectively. Statistical significance was analysed using the unpaired, two-tailed t-test (*p<0.05, **p<0.01).
(F) RT-qPCR analysis for pluripotency-associated gene expression during LIF withdrawal differentiation of both early passage and late passage iPSCs. Results are presented as averages (±SEM) of three male and three female iPSC lines in early passage (P8) and the same lines in late passage (P14), respectively. **p<0.01, ***p<0.001, P8 Female iPSCs vs P8 Male iPSCs. #p<0.05, ##p<0.01, P14 Female iPSCs vs P14 Male iPSCs. Two-way repeated-measures ANOVA with Bonferroni posttests.
(G) qPCR analysis for X-chromosome DNA copy number in both early passage and late passage iPSCs grown in S/L. X copy number are presented as the average ratios of gDNA quantities for four X-linked genes (*Tfe3, Bcor, Pdha1, and Mid1,* locations in X-chromosome shown in lower panel) to gDNA quantities for autosomal gene *Gapdh*.
(H) As in (C) but for male and female iPSC lines in early (P6) and late passage (P13). Growth curve: *p<0.05, ***p<0.001, P6 Female iPSCs vs P6 Male iPSCs; ##p<0.01, ###p<0.001, P13 Female iPSCs vs P13 Male iPSCs; two-way repeated-measures ANOVA with Bonferroni posttests. Td: ***p<0.01, P6 Female iPSCs vs P6 Male iPSCs; ###p<0.001, P13 Female iPSCs vs P13 Male iPSCs; unpaired two-tailed t-test.

Figure 2. Sex-specific chromatin regulatory landscapes in mouse ESCs.

(A) Differential chromatin accessibility analysis between female and male ESCs. Log2 fold change (XX/XY) in reads per accessible region are plotted against the mean reads per ATAC-seq peak. Open chromatin regions that more open in female ESCs or in male ESCs (|log2fold|>=1, false discovery rate (FDR)<=0.05) were defined as “XXgain” and “XYgain”, respectively.
(B) GO analysis of biological processes associated with chromatin more open in female (XXgain) or in male (XYgain) mouse ESCs.
(C) Venn diagrams showing the overlap between genes nearest to the “XXgain” regions and the DEGs between mouse XX and XY ESCs (DEGs= $|\log_2 fold| >= \log_2 1.5$, FDR<=0.05).
(D) Integrated Genome Viewer (IGV) track images of ATAC-seq and RNA-seq signal for “XXgain” example regions. Differentially open regions are shaded.
(E) As in C for “XYgain” regions.
(F) As in D for “XYgain” regions.

Figure 3. Identification of candidate regulators for sex-specific open chromatins.

(A-C) Enriched motifs found in chromatin regions more open in XX ESCs (A), in XY ESCs (C), or both (B).
(D) Venn diagram showing the overlap between the ATAC-seq regions more open in XX ESCs with a motif KLF5, ESRRB and SOX2. The number of genes associated with all three motifs that show increased or decreased expression in XX ESCs is incidtated.
(E) As in D for ATAC-seq regions more open in XY ESCs.

Figure 4. Effects of Zic3 heterozygous deletion on pluripotency exit.

(A) Western blot analysis for ZIC3 (left) in iPSCs and ESCs grown in S/L. Right: quantification using ACTIN as loading control. ZIC3 protein values are represented as averages (±SEM) of male and female iPSC lines (three lines each), and male and female ESC lines (one line each). **p<0.01, Male iPSCs vs Female iPSCs, unpaired two-tailed t-test.
(B) Scheme of heterozygous *Zic3* deletion strategy in female XX ESCs followed by LIF withdrawal.
(C) RT-qPCR analysis for *Zic3* gene expression in two independent *Zic3*+/- ESC lines, *Zic3*+/+ ESCs and XY ESCs all grown in S/L. The expression values are represented as averages (±SEM) of technical duplicates (n=1).
(D) RT-qPCR analysis for pluripotency-associated gene expression during LIF withdrawal in the two independent *Zic3*+/- XX ESC lines, the *Zic3*+/+ XX parental ESC line and a XY ESC line. Results are presented as averages (±SEM) of technical duplicates (n=1).

Figure 5. Transcriptional landscape of female ESCs differentiation in the absence of global DNA hypomethylation.

(A) Scheme of *Dusp9* heterozygous deletion in female XX ESCs followed by LIF withdrawal differentiation.
(B) (i) Western blot analysis for DUSP9, ERK and pERK proteins in *Dusp9*+/- ESCs, *Dusp9*+/+ ESCs and XY ESCs grown in S/L. (ii) Quantification of DUSP9 levels using ACTIN as a loading control and (iii) pERK levels using ERK as a loading control. DUSP9 expression values are represented as averages (±SEM) of the same lines in two independent western blot experiments.
(C) PCA of RNA-seq data for *Dusp9*+/- ESCs, *Dusp9*+/+ ESCs and XY ESCs grown in S/L conditions or 24h after LIF withdrawal. The top 500 most variable genes were used in this analysis.
(D) Unsupervised hierarchical clustering of top 200 most variable genes in *Dusp9*+/- ESCs, *Dusp9*+/+ ESCs and XY ESCs in the undifferentiated state.
(E) Venn diagram showing the overlap between the DEGs of *Dusp9*+/- ESCs with *Dusp9*+/+ ESCs ($|\log_2 fold| >= \log_2 1.5$, FDR<=0.05). The top enriched GO terms for biological processes for common DEGs are shown.
(F) Unsupervised hierarchical clustering of MAPK pathway related genes (defined in [11]) for *Dusp9*+/- ESCs, *Dusp9*+/+ ESCs and XY ESCs in the undifferentiated state.
(G) Unsupervised hierarchical clustering of top 200 most variable genes for *Dusp9*+/- ESCs, *Dusp9*+/+ ESCs and XY ESCs in the differentiated state after 24h of LIF withdrawal.

(H) Expression of *Prdm14* and *Nanog.* RNA-seq data (CPM) for *Dusp9*+/- ESCs, *Dusp9*+/+ ESCs and XY ESCs at 0h and 24h after LIF withdrawal.
(I) RT-qPCR validation of *Prdm14* and *Nanog* expression before and after LIF withdrawal. Results are presented as averages (±SEM) of two independent experiments.
(J) Growth curves and doubling times of *Dusp9*+/- ESCs, *Dusp9*+/+ ESCs and XY ESCs in S/L condition. Cell were counted at the indicated time points and presented as fold changes relative to averages (±SEM) at 0h (n=1).

REFERENCES

1. Avior Y, Sagi I, Benvenisty N. Pluripotent stem cells in disease modelling and drug discovery. Nat Rev Mol Cell Biol. 2016;17: 170–182.

2. Takahashi K, Yamanaka S. Induction of Pluripotent Stem Cells from Mouse Embryonic and Adult Fibroblast Cultures by Defined Factors. Cell. 2006;126: 663–676.

3. Bradley A, Evans M, Kaufman MH, Robertson E. Formation of germ-line chimaeras from embryo-derived teratocarcinoma cell lines. Nature. 1984;309: 255–256.

4. Ying Q-L, Wray J, Nichols J, Batlle-Morera L, Doble B, Woodgett J, et al. The ground state of embryonic stem cell self-renewal. Nature. 2008;453: 519–523.

5. Yagi M, Yamanaka S, Yamada Y. Epigenetic foundations of pluripotent stem cells that recapitulate in vivo pluripotency. Lab Invest. 2017;97: 1133–1141.

6. Schulz EG. X-chromosome dosage as a modulator of pluripotency, signalling and differentiation? Philos Trans R Soc Lond B Biol Sci. 2017;372. doi:10.1098/rstb.2016.0366

7. Ronen D, Benvenisty N. Sex-dependent gene expression in human pluripotent stem cells. Cell Rep. 2014;8: 923–932.

8. Bruck T, Yanuka O, Benvenisty N. Human pluripotent stem cells with distinct X inactivation status show molecular and cellular differences controlled by the X-Linked ELK-1 gene. Cell Rep. 2013;4: 262–270.

9. Zvetkova I, Apedaile A, Ramsahoye B, Mermoud JE, Crompton LA, John R, et al. Global hypomethylation of the genome in XX embryonic stem cells. Nat Genet. 2005;37: 1274–1279.

10. Ooi SK, Wolf D, Hartung O, Agarwal S, Daley GQ, Goff SP, et al. Dynamic instability of genomic methylation patterns in pluripotent stem cells. Epigenetics Chromatin. 2010;3: 17.

11. Schulz EG, Meisig J, Nakamura T, Okamoto I, Sieber A, Picard C, et al. The two active X chromosomes in female ESCs block exit from the pluripotent state by modulating the ESC signaling network. Cell Stem Cell. 2014;14: 203–216.

12. Hackett JA, Dietmann S, Murakami K, Down TA, Leitch HG, Azim Surani M. Synergistic Mechanisms of DNA Demethylation during Transition to Ground-State Pluripotency. Stem Cell Reports. 2013;1: 518–531.

13. Choi J, Clement K, Huebner AJ, Webster J, Rose CM, Brumbaugh J, et al. DUSP9 Modulates DNA Hypomethylation in Female Mouse Pluripotent Stem Cells. Cell Stem Cell. 2017;20: 706–719.e7.

14. Choi J, Huebner AJ, Clement K, Walsh RM, Savol A, Lin K, et al. Prolonged Mek1/2 suppression impairs the developmental potential of embryonic stem cells. Nature. 2017;548: 219–223.

15. Yagi M, Kishigami S, Tanaka A, Semi K, Mizutani E, Wakayama S, et al. Derivation of ground-state female ES cells maintaining gamete-derived DNA methylation. Nature. 2017;548: 224–227.

16. Shirane K, Kurimoto K, Yabuta Y, Yamaji M, Satoh J, Ito S, et al. Global Landscape and Regulatory Principles of DNA Methylation Reprogramming for Germ Cell Specification by Mouse Pluripotent Stem Cells. Dev Cell. 2016;39: 87–103.

17. Mak W. Reactivation of the Paternal X Chromosome in Early Mouse Embryos. Science. 2004;303: 666–669.

18. Maherali N, Sridharan R, Xie W, Utikal J, Eminli S, Arnold K, et al. Directly reprogrammed fibroblasts show global epigenetic remodeling and widespread tissue contribution. Cell Stem Cell. 2007;1: 55–70.

19. Okamoto I, Otte AP, Allis CD, Reinberg D, Heard E. Epigenetic dynamics of imprinted X inactivation during early mouse development. Science. 2004;303: 644–649.

20. Pasque V, Plath K. X chromosome reactivation in reprogramming and in development. Curr Opin Cell Biol. 2015;37: 75–83.

21. Habibi E, Brinkman AB, Arand J, Kroeze LI, Kerstens HHD, Matarese F, et al. Whole-Genome Bisulfite Sequencing of Two Distinct Interconvertible DNA Methylomes of Mouse Embryonic Stem Cells. Cell Stem Cell. 2013;13: 360–369.

22. Milagre I, Stubbs TM, King MR, Spindel J, Santos F, Krueger F, et al. Gender Differences in Global but Not Targeted Demethylation in iPSC Reprogramming. Cell Rep. 2017;18: 1079–1089.

23. Robertson EJ, Evans MJ, Kaufman MH. X-chromosome instability in pluripotential stem cell lines derived from parthenogenetic embryos. J Embryol Exp Morphol. 1983;74: 297–309.

24. Rastan S, Robertson EJ. X-chromosome deletions in embryo-derived (EK) cell lines associated with lack of X-chromosome inactivation. J Embryol Exp Morphol. 1985;90: 379–388.

25. Chen G, Schell JP, Benitez JA, Petropoulos S, Yilmaz M, Reinius B, et al. Single-cell analyses of X Chromosome inactivation dynamics and pluripotency during differentiation. Genome Res. 2016;26: 1342–1354.

26. Carey BW, Markoulaki S, Beard C, Hanna J, Jaenisch R. Single-gene transgenic mouse strains for reprogramming adult somatic cells. Nat Methods. 2010;7: 56–59.

27. De Los Angeles A, Ferrari F, Xi R, Fujiwara Y, Benvenisty N, Deng H, et al. Hallmarks of pluripotency. Nature. 2015;525: 469–478.

28. Burgoyne PS, Thornhill AR, Boudrean SK, Darling SM, Bishop CE, Evans EP. The genetic basis of XX-XY differences present before gonadal sex differentiation in the mouse. Philos Trans R Soc Lond B Biol Sci. 1995;350: 253–60 discussion 260–1.

29. Guo G, Yang J, Nichols J, Hall JS, Eyres I, Mansfield W, et al. Klf4 reverts developmentally programmed restriction of ground state pluripotency. Development. 2009;136: 1063–1069.

30. Pasque V, Tchieu J, Karnik R, Uyeda M, Sadhu Dimashkie A, Case D, et al. X chromosome reactivation dynamics reveal stages of reprogramming to pluripotency. Cell. 2014;159: 1681–1697.

31. Buenrostro JD, Giresi PG, Zaba LC, Chang HY, Greenleaf WJ. Transposition of native chromatin for fast and sensitive epigenomic profiling of open chromatin, DNA-binding proteins and nucleosome position. Nat Methods. 2013;10: 1213–1218.

32. Xu J, Carter AC, Gendrel A-V, Attia M, Loftus J, Greenleaf WJ, et al. Landscape of monoallelic DNA accessibility in mouse embryonic stem cells and neural progenitor cells. Nat Genet. 2017;49: 377–386.

33. Bernstein BE, Mikkelsen TS, Xie X, Kamal M, Huebert DJ, Cuff J, et al. A bivalent chromatin structure marks key developmental genes in embryonic stem cells. Cell. 2006;125: 315–326.

34. Smith A. Formative pluripotency: the executive phase in a developmental continuum. Development. 2017;144: 365–373.

35. Martello G, Smith A. The nature of embryonic stem cells. Annu Rev Cell Dev Biol. 2014;30: 647–675.

36. Okamoto K, Okazawa H, Okuda A, Sakai M, Muramatsu M, Hamada H. A novel octamer binding transcription factor is differentially expressed in mouse embryonic cells. Cell. 1990;60: 461–472.

37. Schöler HR, Dressler GR, Balling R, Rohdewohld H, Gruss P. Oct-4: a germline-specific transcription factor mapping to the mouse t-complex. EMBO J. 1990;9: 2185–2195.

38. Pardo M, Lang B, Yu L, Prosser H, Bradley A, Babu MM, et al. An expanded Oct4 interaction network: implications for stem cell biology, development, and disease. Cell Stem Cell. 2010;6: 382–395.

39. van den Berg DLC, Snoek T, Mullin NP, Yates A, Bezstarosti K, Demmers J, et al. An Oct4-centered protein interaction network in embryonic stem cells. Cell Stem Cell. 2010;6: 369–381.

40. Chen X, Xu H, Yuan P, Fang F, Huss M, Vega VB, et al. Integration of External Signaling Pathways with the Core Transcriptional Network in Embryonic Stem Cells. Cell. 2008;133: 1106–1117.

41. Chambers I, Silva J, Colby D, Nichols J, Nijmeijer B, Robertson M, et al. Nanog safeguards pluripotency and mediates germline development. Nature. 2007;450: 1230–1234.

42. Lim LS, Loh Y-H, Zhang W, Li Y, Chen X, Wang Y, et al. Zic3 is required for maintenance of pluripotency in embryonic stem cells. Mol Biol Cell. 2007;18: 1348–1358.

43. Shaulian E, Karin M. AP-1 as a regulator of cell life and death. Nat Cell Biol. 2002;4: E131–E136.

44. Shaulian E. AP-1 — The Jun proteins: Oncogenes or tumor suppressors in disguise? Cell Signal. 2010;22: 894–899.

45. Yang S-H, Kalkan T, Morrisroe C, Smith A, Sharrocks AD. A genome-wide RNAi screen reveals MAP kinase phosphatases as key ERK pathway regulators during embryonic stem cell differentiation. PLoS Genet. 2012;8: e1003112.

46. Karin M. The Regulation of AP-1 Activity by Mitogen-activated Protein Kinases. J Biol Chem. 1995;270: 16483–16486.

47. Moya IM, Halder G. The Hippo pathway in cellular reprogramming and regeneration of different organs. Curr Opin Cell Biol. 2016;43: 62–68.

48. Tamm C, Böwer N, Annerén C. Regulation of mouse embryonic stem cell self-renewal by a Yes-YAP-TEAD2 signaling pathway downstream of LIF. J Cell Sci. 2011;124: 1136–1144.

49. Roychoudhuri R, Hirahara K, Mousavi K, Clever D, Klebanoff CA, Bonelli M, et al. BACH2 represses effector programs to stabilize T(reg)-mediated immune homeostasis. Nature. 2013;498: 506–510.

50. Jang E, Lee HR, Lee GH, Oh A-R, Cha J-Y, Igarashi K, et al. Bach2 represses the AP-1-driven induction of interleukin-2 gene transcription in CD4＋ T cells. BMB Rep. 2017;50: 472–477.

51. Itoh-Nakadai A, Matsumoto M, Kato H, Sasaki J, Uehara Y, Sato Y, et al. A Bach2-Cebp Gene Regulatory Network for the Commitment of Multipotent Hematopoietic Progenitors. Cell Rep. 2017;18: 2401–2414.

52. Hoshino H, Igarashi K. Expression of the oxidative stress-regulated transcription factor bach2 in differentiating neuronal cells. J Biochem. 2002;132: 427–431.

53. Lim LS, Hong FH, Kunarso G, Stanton LW. The pluripotency regulator Zic3 is a direct activator of the Nanog promoter in ESCs. Stem Cells. 2010;28: 1961–1969.

54. Lee JT, Lu N. Targeted Mutagenesis of Tsix Leads to Nonrandom X Inactivation. Cell. 1999;99: 47–57.

55. Li Z, Fei T, Zhang J, Zhu G, Wang L, Lu D, et al. BMP4 Signaling Acts via dual-specificity phosphatase 9 to control ERK activity in mouse embryonic stem cells. Cell Stem Cell. 2012;10: 171–182.

56. Galupa R, Heard E. X-chromosome inactivation: new insights into cis and trans regulation. Curr Opin Genet Dev. 2015;31: 57–66.

57. Eggan K, Akutsu H, Hochedlinger K, Rideout W 3rd, Yanagimachi R, Jaenisch R. X-Chromosome inactivation in cloned mouse embryos. Science. 2000;290: 1578–1581.

58. Patel S, Bonora G, Sahakyan A, Kim R, Chronis C, Langerman J, et al. Human Embryonic Stem Cells Do Not Change Their X Inactivation Status during Differentiation. Cell Rep. 2017;18: 54–67.

59. Mittwoch U. Blastocysts prepare for the race to be male. Hum Reprod. 1993;8: 1550–1555.

60. Chakraborty D, Paszkowski-Rogacz M, Berger N, Ding L, Mircetic J, Fu J, et al. lncRNA Panct1 Maintains Mouse Embryonic Stem Cell Identity by Regulating TOBF1 Recruitment to Oct-Sox Sequences in Early G1. Cell Rep. 2017;21: 3012–3021.

61. Beddington RS, Robertson EJ. An assessment of the developmental potential of embryonic stem cells in the midgestation mouse embryo. Development. 1989;105: 733–737.

62. Ng RK, Dean W, Dawson C, Lucifero D, Madeja Z, Reik W, et al. Epigenetic restriction of embryonic cell lineage fate by methylation of Elf5. Nat Cell Biol. 2008;10: 1280–1290.

63. Chang G, Gao S, Hou X, Xu Z, Liu Y, Kang L, et al. High-throughput sequencing reveals the disruption of methylation of imprinted gene in induced pluripotent stem cells. Cell Res. 2014;24: 293–306.

64. Yamaji M, Ueda J, Hayashi K, Ohta H, Yabuta Y, Kurimoto K, et al. PRDM14 ensures naive pluripotency through dual regulation of signaling and epigenetic pathways in mouse embryonic stem cells. Cell Stem Cell. 2013;12: 368–382.

65. Chambers I, Colby D, Robertson M, Nichols J, Lee S, Tweedie S, et al. Functional expression cloning of Nanog, a pluripotency sustaining factor in embryonic stem cells. Cell. 2003;113: 643–655.

66. Lin KC, Park HW, Guan K-L. Regulation of the Hippo Pathway Transcription Factor TEAD. Trends Biochem Sci. 2017;42: 862–872.

67. Ying Q-L, Nichols J, Evans EP, Smith AG. Changing potency by spontaneous fusion. Nature. 2002;416: 545–548.

68. Branco MR, King M, Perez-Garcia V, Bogutz AB, Caley M, Fineberg E, et al. Maternal DNA Methylation Regulates Early Trophoblast Development. Dev Cell. 2016;36: 152–163.

69. Fulco CP, Munschauer M, Anyoha R, Munson G, Grossman SR, Perez EM, et al. Systematic mapping of functional enhancer-promoter connections with CRISPR interference. Science. 2016;354: 769–773.

70. Silva J, Nichols J, Theunissen TW, Guo G, van Oosten AL, Barrandon O, et al. Nanog Is the Gateway to the Pluripotent Ground State. Cell. 2009;138: 722–737.

71. Chen Y, Lun ATL, Smyth GK. From reads to genes to pathways: differential expression analysis of RNA-Seq experiments using Rsubread and the edgeR quasi-likelihood pipeline. F1000Res. 2016;5: 1438.

72. Heberle H, Meirelles GV, da Silva FR, Telles GP, Minghim R. InteractiVenn: a web-based tool for the analysis of sets through Venn diagrams. BMC Bioinformatics. 2015;16: 169.

73. Lee J, Christoforo G, Christoforo G, Foo CS, Probert C, Kundaje A, et al. kundajelab/atac_dnase_pipelines: 0.3.3 [Internet]. 2016. doi:10.5281/zenodo.211733

74. Zhang Y, Liu T, Meyer CA, Eeckhoute J, Johnson DS, Bernstein BE, et al. Model-based analysis of ChIP-Seq (MACS). Genome Biol. 2008;9: R137.

75. Stark R, Brown G. DiffBind: differential binding analysis of ChIP-Seq peak data. R package version. bioconductor.statistik.tu-dortmund.de; 2011; Available: https://bioconductor.statistik.tu-dortmund.de/packages/2.13/bioc/vignettes/DiffBind/inst/doc/DiffBind.pdf

76. McLean CY, Bristor D, Hiller M, Clarke SL, Schaar BT, Lowe CB, et al. GREAT improves functional interpretation of cis-regulatory regions. Nat Biotechnol. 2010;28: 495–501.

77. Heinz S, Benner C, Spann N, Bertolino E, Lin YC, Laslo P, et al. Simple combinations of

1 lineage-determining transcription factors prime cis-regulatory elements required for
2 macrophage and B cell identities. Mol Cell. 2010;38: 576–589.

3

Figure 1

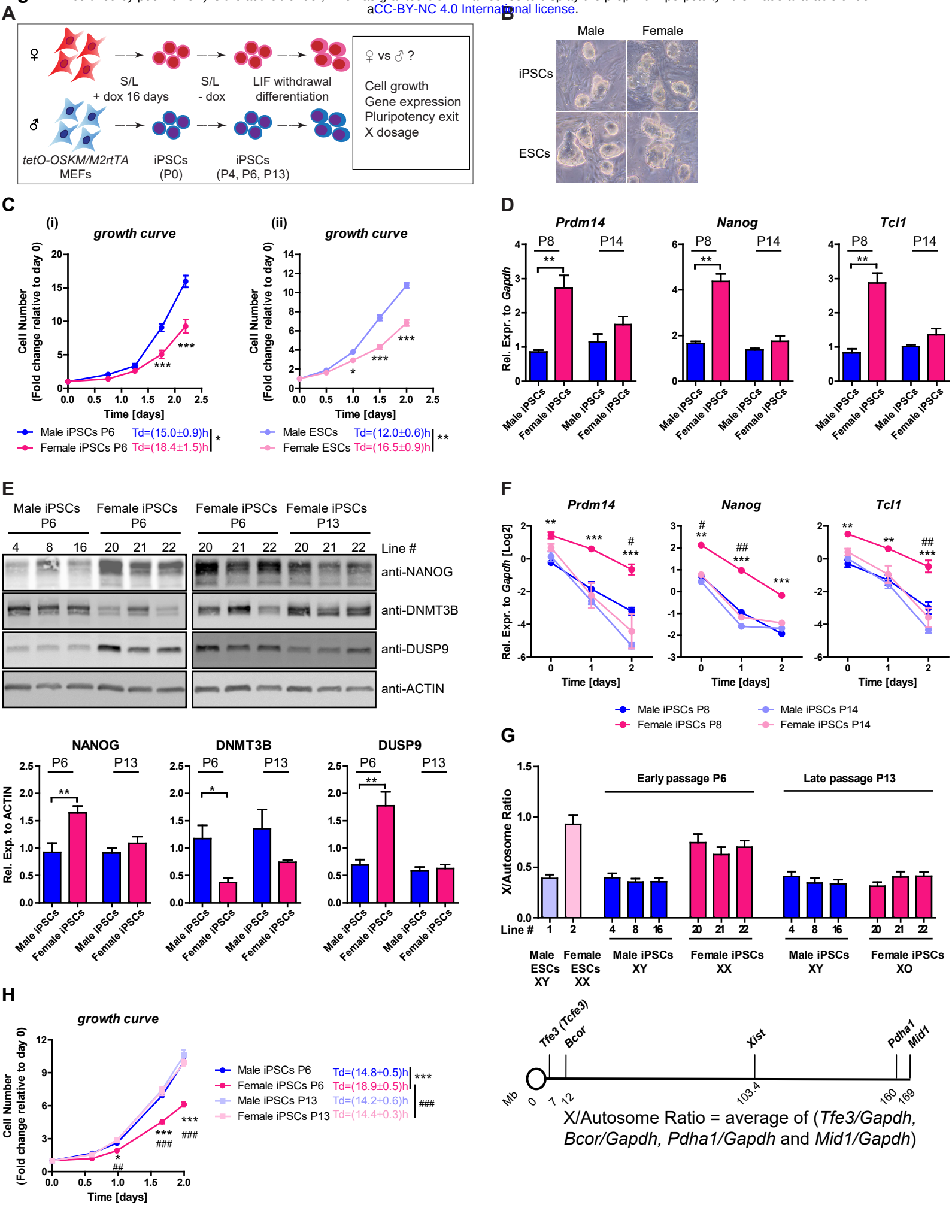

Figure 2

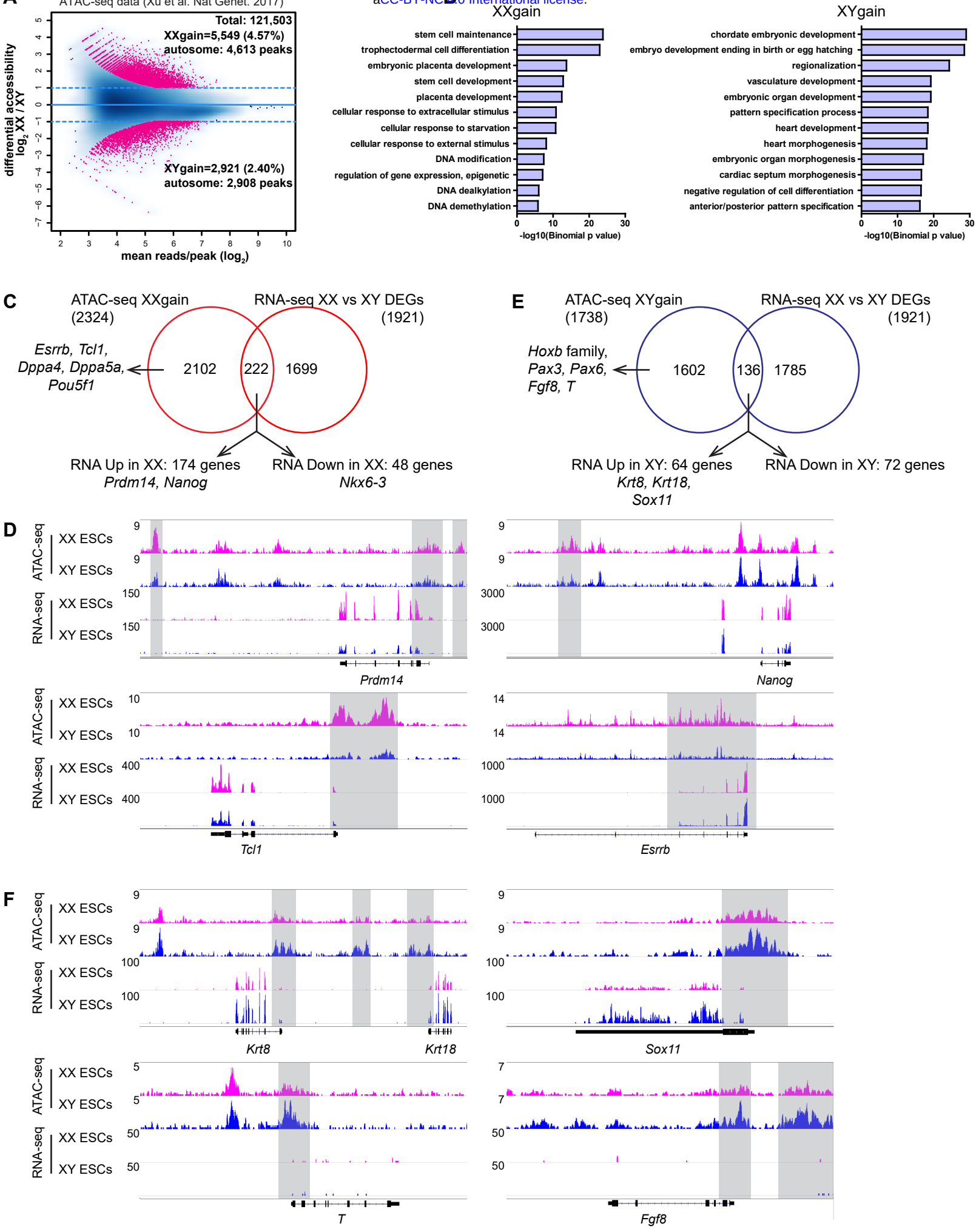

Figure 3

A XXgain:4613 peaks

Motif	Name	p-value	% of targets with Motif
	KLF5	1e-417	61.52%
	ESRRB	1e-202	35.33%
	SOX3	1e-172	58.44%
	OCT4-SOX2-TCF-NANOG	1e-171	13.18%
	SOX2	1e-170	37.59%
	ZIC3	1e-58	24.00%

C XYgain: 2908 peaks

Motif	Name	p-value	% of targets with Motif
	JUN-AP1	1e-172	18.99%
	TEAD	1e-166	32.78%
	FRA2	1e-159	26.18%
	BACH2	1e-73	12.38%

B

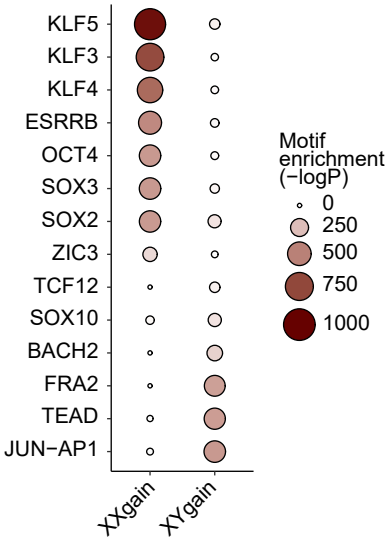

D

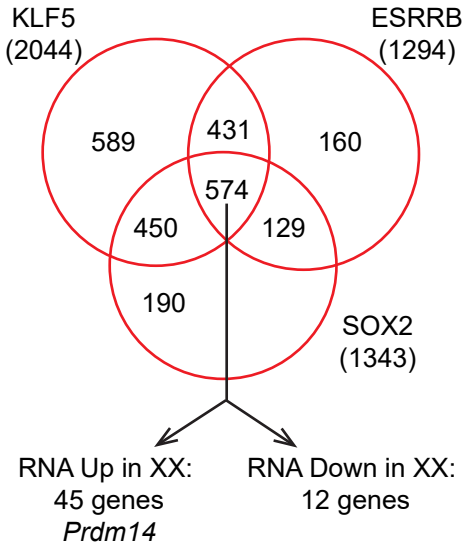

E

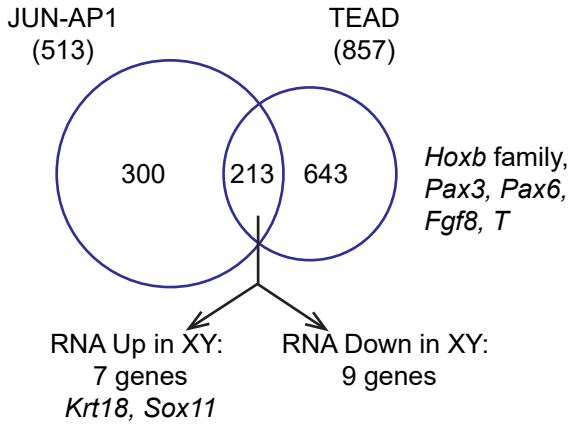

Figure 4

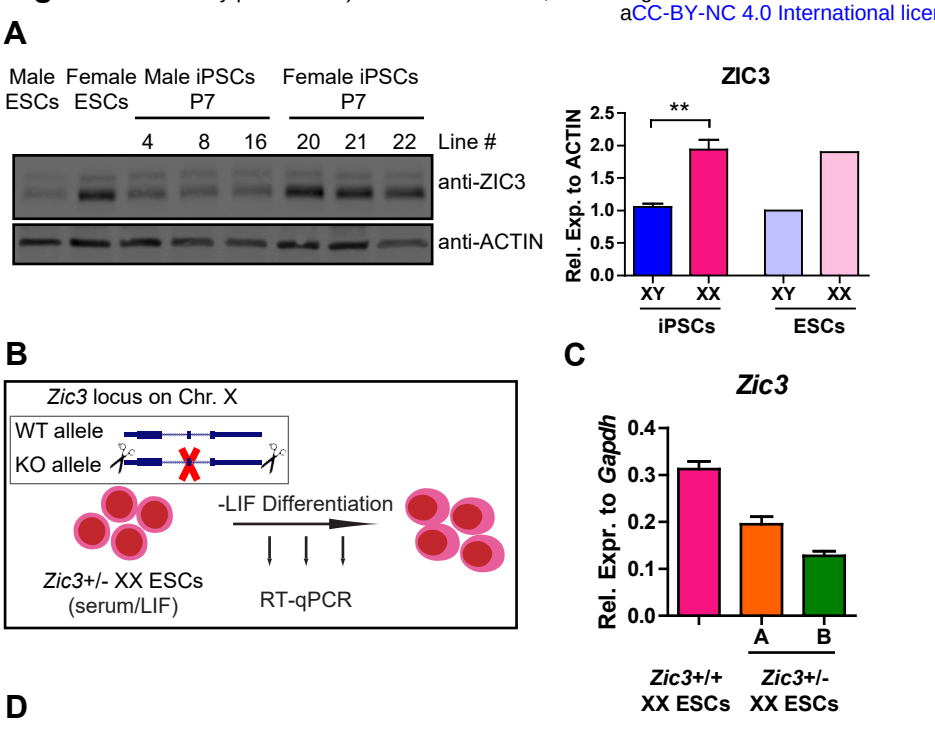

Figure 5